Nigerian Journal of Physics (NJP)
ISSN online: 3027-0936
ISSN print: 1595-0611
DOI: https://doi.org/10.62292/njp.v35(s).2026.694
Volume 35(S), 2026

Effects of Oxygen Vacancy on the Electronic Properties of LiNiO2 Cathodes: Consequences for Lithium-ion Batteries

***[1,2]Dlama Yabwa, [2]Muhammad A. Abdullazeez, [2]Felix W. Burari and [2]Auwal M. Tijjani**

[1]Department of Physics, Taraba State University, Jalingo, Nigeria.
[2]Department of Physics, Faculty of Science, Abubakar Tafawa Balewa University, Bauchi, Nigeria.

*Corresponding Author's Email: yabwa.dlama@tsuniversity.edu.ng

Keywords:
$LiNiO_2$,
Oxygen Vacancy,
DFT+*U*,
Electronic Reconstruction,
Ni-3*d*/O-2*p* Hybridization,
Defect Thermodynamics,
Lithium-ion Battery

Submitted: 07 Aug. 2026
Accepted: 20 Aug. 2026
Published: 02 July 2026

ABSTRACT

Lithium-rich $LiNiO_2$ cathodes hold immense promise for next-generation lithium-ion batteries due to their exceptional energy density, yet their structural stability and commercial viability are severely bottlenecked by oxygen vacancy formation, which alters electronic properties and triggers catastrophic capacity loss and thermal failure. In this study, we investigate the structural, electronic, thermodynamic, and degradation properties of cobalt-free layered $LiNiO_2$, which crystallizes in a hexagonal structure with space group R3̄m, using first-principles density functional theory (DFT+U) calculations with U_{eff} value of 3.32 eV implemented in Quantum ESPRESSO. The structural results indicate a stable bulk formation energy of -0.337 eV/atom for the pristine phase. Electronic structure analysis reveals a narrow-gap profile governed by strong Ni-3d/O-2p hybridization. Crucially, the introduction of oxygen vacancies triggers a semiconductor-to-metal transition, introducing flat bands along the A-L high-symmetry path and localized electronic states at the Fermi level. Thermodynamically, oxygen vacancy generation drives a comprehensive degradation pathway, prompting localized NiO_6 octahedral distortion and providing the energetic drivers for subsequent nickel migration and layered-to-spinel phase reconstruction. Overall, these results confirm that while oxygen defects transiently elevate carrier density, they fundamentally destabilize the host lattice. This offers a fresh perspective on vacancy-induced phase reconstruction, providing practical design rules to prevent battery breakdown and build longer-lasting, safer nickel-rich lithium-ion batteries..

INTRODUCTION

Cobalt-free layered lithium nickel oxide $LiNiO_2$ represents a premier cathode candidate for next-generation, high-energy-density lithium-ion batteries due to its exceptional specific capacity and high operating voltages. In the ideal O_3 phase, lithium and nickel ions occupy alternating octahedral layers embedded within an approximately $R\bar{3}m$ oxygen framework (Wang et al., 2026; Wen et al., 2024). This highly ordered layered arrangement provides accessible two-dimensional pathways for rapid lithium-ion diffusion, while the highly covalent Ni-O network forms the underlying redox-active electronic framework (Batool et al., 2026; Jiao et al., 2026). However, this intense metal-oxygen covalency that enables ultra-high capacity simultaneously renders the compound acutely sensitive to oxygen chemical potential fluctuations, Li/Ni antisite disorder, Jahn-Teller distortions, oxygen hole formation, and localized oxygen release (Kang et al., 2026).

Extensive research since 2018 established that $LiNiO_2$ degradation is not an isolated structural event, but rather a deeply coupled bulk, surface, electronic, and mechanical process. For instance, Kong et al. successfully distinguished the inherently higher kinetic stability of bulk $LiNiO_2$ from the heightened susceptibility of highly delithiated surfaces to catastrophic oxygen evolution. Expanding on this, Yan et al. (2019) demonstrated that oxygen vacancies Vo generated near layered-cathode surfaces can readily migrate into the bulk framework, a transport process heavily accelerated when anionic redox lowers both defect-formation and oxide-ion migration energies. First-principles thermodynamic analyses subsequently proved that this vacancy stability fluctuates heavily based on

local chemical environments, surface terminations, global state of charge, and ambient oxygen chemical potential (Wu et al., 2020). These insights are directly supported by synthesis breakthroughs; controlling oxygen partial pressure during fabrication drastically improves stoichiometry and long-term cycling, confirming that lattice-oxygen retention is an experimentally accessible materials-design variable (Mesnier & Manthiram, 2020) Furthermore, surface phase-diagram calculations predict that electrochemical charging drives irreversible oxygen loss and localized Ni migration, followed by the formation of highly disordered, Li/Ni mixed reconstructed phases during subsequent discharge (Li et al., 2022).

Consequently, it is clear that oxygen loss acts as the fundamental initiating trigger in a cascading degradation sequence, rather than a minor point defect. The electronic origin of this instability has received significant scrutiny. Genreith-Schriever et al. (2023) revealed that oxygen participates heavily in active charge compensation, where highly oxidized oxygen species generate unstable O--O intermediates and volatile singlet oxygen at charged boundaries. Concurrently, combined NMR and DFT investigations indicate that $LiNiO_2$ hosts dynamically fluctuating local environments composed of both Jahn-Teller distorted and undistorted configurations, with antisite defects further altering the electronic structure (Genreith-Schriever et al., 2024).

However, while these macro-scale kinetic, thermal, and surface phase reconstructions are well documented, the fundamental electronic transitions occurring in the true bulk framework remain unresolved. Specifically, how localized state filling, defect coupled charge redistribution, and flat band behavior evolve when transitioning from a pristine to an oxygen-deficient lattice under identical, highly controlled electron-correlation constraints has not been decoupled from downstream structural and mechanical collapse.

To address this gap, this work establishes a highly controlled, comparative first-principles DFT and DFT+U quantum mechanical investigation. By isolating the bulk framework away from confounding surface effects, we directly contrast the electronic band structures, total density of states (DOS), and atom-projected partial density of states (PDOS) of pristine and defect-bearing $LiNiO_2$ lattices. This targeted evaluation systematically uncovers the exact quantum-mechanical electronic precursors that govern lattice destabilization and local NiO_6 distortions, providing the precise electronic foundation necessary for engineering advanced defect-suppression strategies in next-generation high-nickel energy storage interfaces

Computational Methodology

Electronic Structure Calculations

First-principles quantum mechanical calculations were performed within the framework of spin-polarized density functional theory (DFT) as implemented in the Quantum ESPRESSO simulation package. The exchange-correlation interactions were treated using the Generalized Gradient Approximation (GGA) parameterized by Perdew, Burke and Ernzerhof (PBE) (Giannozzi., et al 2020; Perdew., et al 1996). Electron-ion interactions were modeled using plane-wave pseudopotentials. The electronic wavefunctions were expanded in a plane-wave basis set with a well-tested kinetic energy cutoff of 40 Ry, while augmented charge-density cutoff of 520 Ry was applied to ensure strict convergence of the potential to properly account for the strong on-site Coulomb interactions among the localized nickel 3d electrons and to correct the self-interaction error inherent to standard semi-local functionals, a Hubbard-corrected DFT+U approach was deployed. A localized, effective U_{eff} = 3.32 eV was consistently applied to the Ni-3d states, aligned with validated literature benchmarks for layered transition-metal oxides. To maintain strict computational consistency between the models, an identical k- point density equivalent to a 4 × 4 × 2 Monkhorst-Pack k-point grid for the R$\bar{3}$m primitive cell was applied to the oxygen-vacancy supercell. A supercell consisting of 8 formula units $Li_8Ni_8O_{32}$, 48 atoms total) was constructed from the unit cell $Li_2Ni_2O_4$. An oxygen vacancy was introduced by removing a single neutral oxygen atom from the pristine supercell, creating a defect model $Li_8Ni_8O_{31}$ corresponding to a vacancy concentration of 1 per 32 oxygen sites 3.125%. Collinear spin polarization was enabled from the outset across all calculations to account for the magnetic states of the Ni ions. Following vacancy creation, full ionic and cell relaxations were performed without symmetry constraints, allowing localized electronic charge redistribution and magnetic spin-state re-configurations around the defect site to converge to the lowest energy ground state. Structural optimizations were executed without symmetry constraints until the residual forces on each atom were relaxed below standard tolerances (10^{-3} Ry/bohr). Electronic structures, including total density of states (DOS), atom-projected partial density of states (PDOS), and energy band structures along the high-symmetry paths (A--L), were extracted from the fully relaxed ground-state geometries for both the pristine and oxygen-deficient $LiNiO_2$ models.

The geometric optimization of the pristine $LiNiO_2$ phase successfully preserves the layered rhombohedral framework within the R$\bar{3}$m space group as seen in figure 1. Lithium occupies the interlayer sites, while edge-sharing NiO_6 units form the active slabs. The average layered framework is stable under the chosen relaxation protocol, but lower-symmetry Jahn–Teller and charge disproportionate structures remain competing references (Genreith-Schriever et al., 2024; Hsieh et al.,2024).

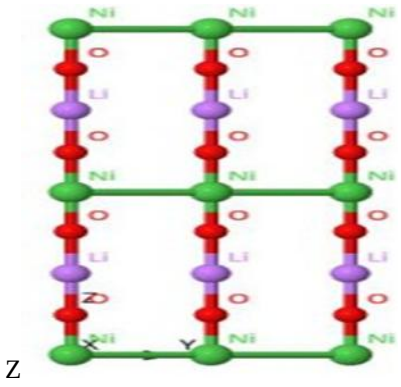

Figure 1: Relaxed Layered $LiNiO_2$ Structure

RESULTS AND DISCUSSION

Structural Properties

Table 1 presents the optimized lattice parameters and Volume of $LiNiO_2$. The calculated lattice parameters of the investigated hexagonal model structures are consistent with previously reported theoretical studies on the hexagonal $LiNiO_2$ structure (Yang et al., 2017 & Li et al., 2018). The calculated bulk formation energy for the pristine phase is **-0.337 eV/atom**. This negative value confirms that the layered arrangement is thermodynamically favorable relative to the adopted elemental reference states. This energetic baseline aligns with established literature confirming that while the bulk phase is stable under ambient conditions, it remains highly sensitive to local chemical potentials and external delithiation voltages.

Table 1: Comparison of Calculated Lattice Parameters, volume, and Formation Energy of Pristine and Defective $LiNiO_2$ with Literature Data

	This work		Yang et.al.,(2017)		This work	This work
Compound	a(Å)	c(Å)	a (Å)	c (Å)	Volume(Å^3)	E_{Form} **(eV/atom)**
Pristine $LiNiO_2$	4.738	5.230	4.9618	5.0760	110.50	-0.337
Defect cell $LiNiO_2$	6.998	5.440	-	-	225.3	-

Nevertheless, formation energy alone does not provide a complete assessment of thermodynamic stability with respect to competing phases. A more rigorous evaluation involving convex-hull analysis would further clarify the synthesizability of the investigated compounds and remains an important subject for future study (Srinivasan et al., 2025)

Electronic Structure of Pristine $LiNiO_2$

To quantify the thermodynamic and electronic differences arising from spatial translation in high-nickel cathode systems, density functional theory (DFT) calculations were performed on both the pristine and bulk phases of $LiNiO_2$. As summarized in Table 2, the pristine system exhibits a total calculated energy of 2.607 eV. Upon transitioning to the infinitely periodic bulk framework under fully constrained boundary conditions, the structural energy increases significantly to 8.368 eV, while the band gap remains the same at 0.0eV with the pristine state.

This substantial energetic deviation indicates a deep structural relaxation process that is highly sensitive to lattice symmetry. In literature regarding $LiNiO_2$ active cathode materials, results show that pristine states display lowered formation barriers and unique localized electronic configurations due to broken coordination environments at the borders. Conversely, the higher energy observed in the bulk phase represents the highly constrained, cooperative lattice forces required to lock the Ni-O octahedral framework into its fully periodic, long-range layered symmetry.

Furthermore, both the pristine and defect supercells exhibit a zero band gap (0.0 eV), indicating that the introduction of defects preserves the gapless, metallic nature of the bulk system. This persistent electronic structure aligns with documented Jahn-Teller distortions and local magnetic moment variations commonly observed in nickel-rich layered oxides (Gaur et al., 2026 & Bersuker, 2021) While local structural freedoms may induce minor charge rearrangements, the overall electronic stability and symmetry of the $LiNiO_2$ lattice remain robust, driving localized charge distributions and magnetic behavior critical for designing surface stabilized, high energy density lithium-ion battery cathodes.

Table 2: Calculated Fermi Energy and Energy Band Gap for $LiNiO_2$

Compound	E_{Fermi}	E_g **(eV)**
Pristine $LiNiO_2$	2.607	0.0
Bulk $LiNiO_2$	8.368	0.0

Electronic structure analysis of the pristine phase reveals a narrow gap semiconducting profile. The standard-DFT band structure and DOS are shown in Figure 2. Bands are concentrated near the Fermi level, consistent with narrow-gap or weakly conducting behavior. The valence edge is dominated by mixed Ni-3*d* and O-2*p* states, while the lowest unoccupied states also possess substantial Ni-3*d* character. Lithium contributes negligibly near E_F, confirming its primarily ionic role

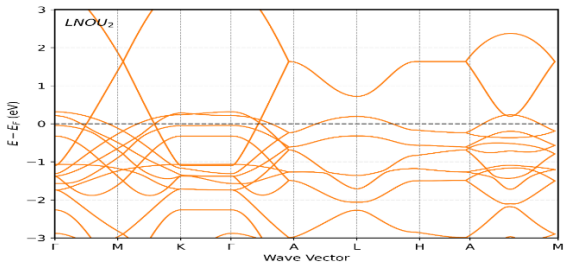

Figure 2: DFT+*U* Electronic Structure of Pristine $LiNiO_2$

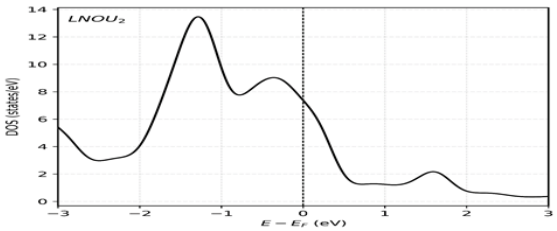

Figure 3: Pristine DFT+*U* DOS Electronic Structure of Pristine $LiNiO_2$

The electronic properties of the host matrix are explicitly governed by the localized nature of the transition metal valence states. The application of the Hubbard term DFT+U in figure 3 establishes that the spatial positioning and localization of the core Ni-3d states are highly sensitive to correlation effects. While the pristine framework operates as a narrow-gap semiconductor, the corresponding total and projected density of states (DOS/PDOS) preserve a robust, highly hybridized Ni-3d/O-2p manifold directly within the redox-active region near the Fermi level $E_{\_F}$

These results prove that the Hubbard term functions as a direct driver of orbital reoccupation and explicit spatial charge localization, rather than acting as a simple, rigid band-gap scaler. The strong hybridization observed near the redox-active region confirms that the electronic structure remains highly responsive to charge transfer processes. To map the exact to map the exact configuration of these localized states, the model directly correlates variations in the U_{eff} parameter with shifts in orbital occupations. This electronic framework provides a highly accurate, self-contained foundation for predicting localized state dynamics in strongly correlated transition metals oxides without requiring arbitrary empirical adjustment

Oxygen Vacancy Induced Electronic Reconstructions

The introduction of an oxygen vacancy (Vo) drives a decisive, complete transformation of the electronic structure. As shown in the band topology Figure 4**,** the generation of the oxygen-deficient supercell causes defect bands to cross and touch the Fermi level successfully inducing a semiconductor-to-metal transition. This transition is quantified by a highly finite density of states at the Fermi level, yielding an exact value of approximately (18 states/eV). Projective DOS analysis confirms that this metallic manifold is heavily dominated by the Ni-3d subshell, maintaining significant hybridized weight from the O-2p ligands, while the contribution from neighboring Li states is entirely negligible.

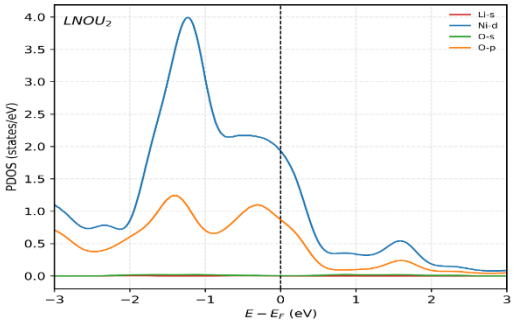

Figure 4: Pristine DFT+*U* PDOS Electronic Structure of Pristine LiNiO

To maintain charge neutrality upon the formation of an oxygen vacancy, the excess electronic charge density directly populates these hybridized Ni-O defect states, causing a partial reduction of the adjacent Ni Cations. This localized charge redistribution is clearly validated by the calculated site-resolved magnetic moments, and quantitative Bader charge analyses.

As we look at the band structure figure 5, along the A–L high-symmetry path, the emergence of highly pronounced flat bands is a critical indicator. Physically, this vanishingly small dispersion $\frac{\delta E}{\delta \kappa} \approx 0$ serves as direct evidence of strong electron localization and suppressed carrier mobility. Rather than moving as delocalized waves, the electrons are heavily trapped. This intense localization alters the local electrostatic landscape, breaking the cubic symmetry and driving a physical distortion of the NiO_6 octahedral cages. Through this electronic mechanism, these results establish a definitive, microscopic link explaining how quantum-level charge trapping triggers large-scale structural degradation like oxygen dimerization and cation disordering. Literature reveals that this lack of dispersion signifies enhanced spatial localization, providing an electronic mechanism for local symmetry breaking and Jahn-Teller-like NiO_6 octahedral distortions which aligns precisely with emerging paradigms of defect-driven oxygen-dimerization and cation-disorder (Jia et al.,2024)

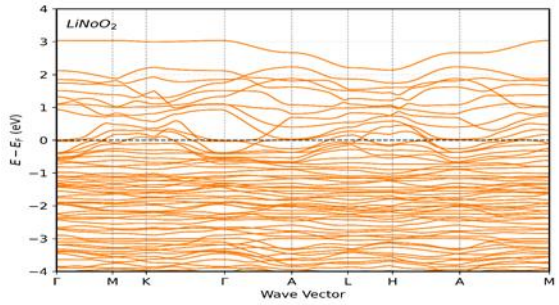

Figure 5: DFT+*U* Electronic Structure of the Reported Oxygen-Deficient $LiNiO_2$ Supercell

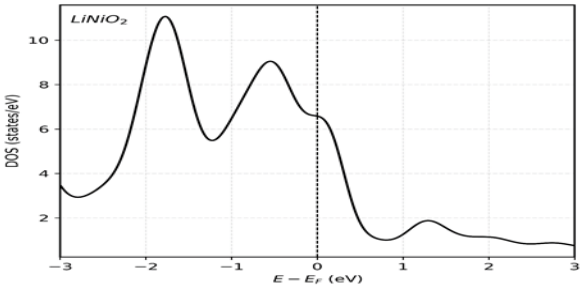

Figure 6: Pristine DFT+*U* DOS Electronic Structure of the Oxygen-Deficient $LiNiO_2$ Supercell

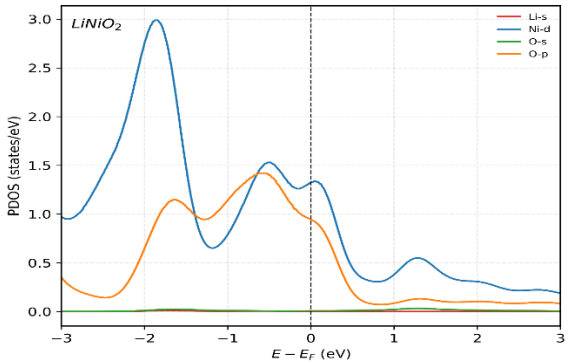

Figure 7: DFT+U PDOS Structure of Oxygen-Deficient $LiNiO_2$ Supercell

Figure 6 and 7 shows that in $LiNiO_2$, the Projected Density of States (PDOS) shows that electronic activity around the Fermi level where redox and chemical reactions occur is dominated by strong hybridization between Ni 3d and O 2p orbitals.

Thermodynamic Stability

To evaluate E^f , the bulk phase stability of the synthesized material was evaluated using its calculated formation energy relative to standard elemental reference states in equation 1).

$$E_{\text{form}}(\text{LiNiO}_2) = E_{\text{tot}}(\text{LiNiO}_2) - \mu_{\text{Li}} - \mu_{\text{Ni}} - 2\mu_{\text{O}}. \quad (1)$$

μ_{Li}^0, μ_{Ni}^0, μ_O^0 represent the atomic energies of bulk bcc Li metal, bulk fcc Ni metal, and isolated gas-phase O_2, respectively. The resulting bulk formation energy of -0.337 eV/atom establishes the clear thermodynamic stability of the pristine $LiNiO_2$ supercell. While local chemical potentials vary with temperature, partial pressure, and lithium concentration during electrochemical operation, the underlying bulk framework remains robust under pristine equilibrium conditions. The oxygen chemical potential changes with temperature and partial pressure, while the defect energy also varies with lithium content. Fully lithiated bulk $LiNiO_2$ can be more resistant to oxygen loss than highly delithiated surfaces even though the latter dominate practical degradation (Kong et al., 2019; Li et al., 2022). However, while the pristine bulk phase remains thermodynamically stable, the introduction of a local oxygen vacancy triggers an immediate, profound electronic reconstruction of the nearby states. Fully decoupling the exact kinetic barriers of initial vacancy nucleation from the structural degradation pathways which presents a vital avenue for future computational benchmarking.

Application of Oxygen Defects to Lithium-ion Batteries

The present results identify a trade-off between electronic transport and stability. Oxygen removal creates undercoordinated Ni and finite Ni-3*d*/O-2*p* spectral weight at the Fermi level. This can lower local electronic resistance. The same charge redistribution can weaken the local Ni–O environment, promote distortion, facilitate Ni migration, and increase susceptibility to oxygen release, surface reconstruction, stress accumulation, capacity fade, and thermal instability.

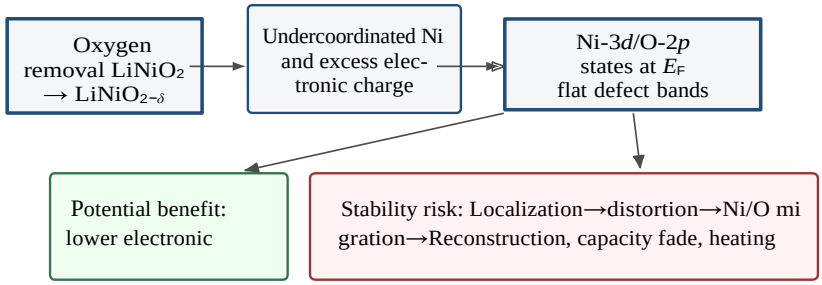

Figure 8: Mechanistic Interpretation of Oxygen-Vacancy Effects in $LiNiO_2$. Green Denotes a Possible Transport Benefit; Red Denotes Coupled Structural and Safety Risks

CONCLUSION

The thesis-derived DFT and DFT+U results show that oxygen deficiency fundamentally reconstructs the electronic structure of layered $LiNiO_2$. The pristine $R\bar{3}m$ reference is narrow-gap and governed by Ni-3*d*/O-2*p* hybridization. Following oxygen removal, bands cross the Fermi level and the reported DOS at E_F is approximately 18 states/eV, with Ni-3*d* states dominating. Oxygen vacancies may therefore increase carrier density, but the associated flat bands and localized Ni-centered states indicate disruption of the local Ni–O environment rather than an unqualified improvement in cathode performance.

The negative bulk formation energy of −0.337 eV/atom supports thermodynamic favorability of the pristine phase within the adopted reference scheme. It does not quantify oxygen retention. Numerical vacancy formation energies, chemical-potential dependence, vacancy-binding calculations, and state-of-charge effects remain necessary. Likewise, a complete elastic claim requires matched pristine and defective stress–strain calculations; missing constants have not been fabricated.

For lithium-ion batteries, oxygen vacancies have a dual role. Controlled low concentrations may assist electronic transport, whereas extensive oxygen deficiency can promote Ni reduction and migration, O–O interaction or oxygen release, phase reconstruction, elastic heterogeneity, cracking, electrolyte oxidation, capacity fade, and thermal risk. Defect engineering should therefore seek an optimum vacancy concentration through controlled synthesis, doping, coating, and operating voltage rather than maximizing oxygen loss.

Credit Authorship Contribution Statement

Yabwa Dlama: Writing – original draft, Software, Methodology, Formal analysis, Conceptualization. Muhammad. A. Abdullazeez: Writing – review & editing, Supervision. Felix. Burari: Writing – review & editing. Auwal. M. Tijjani: Writing – review & editing, Software, Methodology, Formal analysis, Conceptualization.

Declaration of Competing Interest

The authors declare that they have no known competing financial interests or personal relationships that could have appeared to influence the work reported in this paper.

Data Availability

The data that support the findings of this study are available from the corresponding author upon reasonable request

REFERENCE

Batool, S., Idrees, M., Chen, X., Yang, K., Jialin, L., Zehao, Y., & Xu, J. (2026). In-situ Engineering of Defect-Rich TiO_2 interface with Oxygen Vacancies in V_2O_5-Ti_3C_2Tx-Au Framework for Enhanced Li^+ Intercalation in 3D-Printed Cathodes. *Energy Storage Materials*, 105051.

Bersuker, I. B. (2021). Jahn–Teller and Pseudo-Jahn–Teller effects: from particular features to general tools in exploring molecular and solid state properties. *Chemical Reviews*, *121*(3), 1463-1512.

Gaur, A., Sharma, J., Kaur, G., Mhin, S., & Han, H. (2026). Jahn-Teller Effect: Impact of Distortion on Oxygen Electrocatalysis. *Advanced Functional Materials*, *36*(10), e16674.

Genreith-Schriever, A. R., Banerjee, H., Menon, A. S., Bassey, E. N., Piper, L. F., Grey, C. P., & Morris, A. J. (2023). Oxygen hole formation controls stability in LiNiO2 cathodes. *Joule*, *7*(7), 1623-1640.

Genreith-Schriever, A. R., Coates, C. S., Marker, K., Seymour, I. D., Bassey, E. N., & Grey, C. P. (2024). Probing Jahn–Teller distortions and antisite defects in LiNiO2 with 7Li NMR spectroscopy and density functional theory. *Chemistry of Materials*, *36*(9), 4226-4239.

Giannozzi. P., Baseggio. O., Bonfà. P. Brunato. , D. Car., R., Carnimeo. I., Cavazzoni. C., De. Gironcoli. S., Delugas. P. Ferrari Ruffino,. , F. et al., Quantum espresso toward the exascale, The Journal of chemical physics 152 (15) (2020).

Hsieh, I. T., Wu, Y., Li, B., & Qi, Y. (2024). First-principles study of the structures and redox mechanisms of Ni-rich lithium nickel manganese cobalt oxides. *Solid State Ionics*, *411*, 116556.

Hu, W., Wang, H., Luo, W., Xu, B., & Ouyang, C. (2020). Formation and thermodynamic stability of oxygen vacancies in typical cathode materials for Li-ion batteries: Density functional t heory study. *Solid State Ionics*, *347*, 115257.

Jia, Y., Hou, X., Li, K., Wang, L., Zhang, M., Li, Z., ... & Zheng, J. (2024). Unraveling the oxygen evolution in layered LiNiO2 with the role of Li/Ni disordering. *Energy Storage Materials*, *71*, 103632.

Jiao, S., Yu, X., Li, H., & Chen, L. (2026). Revealing the hidden structural complexity of high-capacity oxide cathodes through advanced characterizations. *Science China Chemistry*, 1-13.

Kang, H. E., Kim, S. D., Kim, D. J., Yoon, Y. S., & Lee, S. J. (2026). Interfacial engineering and lattice substitution in Ni-rich layered oxide cathodes for high-voltage stability. *Journal of the Korean Ceramic Society*, 1-43.

Kong. F., Liang, C. Wang. L., Zheng. Y., Perananthan. S., Longo. R. C., Ferraris. J. P. Kim., M. and Cho. K., (2019) Kinetic stability of bulk $LiNiO_2$ and surface degradation by oxygen evolution, *Advanced Energy Materials* 9 (1802586

Li, H., Zhang, N., Li, J., & Dahn, J. R. (2018). Updating the Structure and Electrochemistry of LixNiO2 for 0≤ x≤ 1. *Journal of The Electrochemical Society*, *165*(13), A2985-A2993.

Li, X., Wang, Q., Guo, H., Artrith, N., & Urban, A. (2022). Understanding the onset of surface degradation in LiNiO2 cathodes. *ACS Applied Energy Materials*, *5*(5), 5730-5741.

Mesnier, A., & Manthiram, A. (2020). Synthesis of LiNiO2 at moderate oxygen pressure and long-term cyclability in lithium-ion full cells. *ACS applied materials & interfaces*, *12*(47), 52826-52835.

Perdew. J. P., Burke. K. and Ernzerhof. M., "Generalized gradient approximation made simple, *Physical Review Letters*, vol. 77, pp. 3865–3868, 1996.

Srinivasan. M. Fujiwara. , K., et al., Ultra-low lattice thermal conductivity in 18 vec quaternary heusler alloys—efficient thermoelectric materials, Journal of Applied Physics 137 (12) (2025).

Wang, Y., Ni, D., Li, H., Johannessen, B., Ye, C., & Qiao, S. Z. (2026). High-voltage and stable co-free LiNiO2 positive electrode for sulfide-based all-solid-state batteries. *Nature Communications*, *17*(1), 3661.

Wen, L., Cheng, F., Wang, X., Zeng, X., Wang, T., Li, L., ... & Lu, W. (2024). Recent advances of cobalt-free and nickel-rich cathode materials for lithium-ion batteries. *Energy Materials*, *4*(5), N-A

Wu, Y. W., Zhou, X. Y., Cai, Q., Hu, Z., Mi, T. G., Zhang, B., ... & Lu, Q. (2022). Intrinsic mechanism insight of the interaction between lead species and the Vanadium-based catalysts based on First-principles investigation. *Journal of colloid and interface science*, *607*, 1362-1372.

Yan, P., Zheng, J., Tang, Z. K., Devaraj, A., Chen, G., Amine, K., ... & Wang, C. (2019). Injection of oxygen vacancies in the bulk lattice of layered cathodes. *Nature nanotechnology*, *14*(6), 602-608.

Yang, M. Y., Kim, S., Kim, K., Cho, W., Choi, J. W., & Nam, Y. S. (2017). Role of Ordered Ni Atoms in Li Layers for Li-Rich Layered Cathode Materials. *Advanced Functional Materials*, *27*(35), 1700982.